7-2012

On Establishing Elastic–Plastic Properties of a Sphere by Indentation Testing

J. K. Phadikar
University of Delaware

T. A. Bogetti
University of Delaware

Anette M. Karlsson
Cleveland State University, a.karlsson@csuohio.edu

Publisher's Statement

NOTICE: this is the author's version of a work that was accepted for publication in International Journal of Solids and Structures. Changes resulting from the publishing process, such as peer review, editing, corrections, structural formatting, and other quality control mechanisms may not be reflected in this document. Changes may have been made to this work since it was submitted for publication. A definitive version was subsequently published in International Journal of Solids and Structures, 49, 14, (07-01-2012); 10.1016/j.ijsolstr.2012.04.001

Original Citation

Phadikar, J. K., Bogetti, T. A., and Karlsson, A. M., 2012, "On Establishing elastic–plastic Properties of a Sphere by Indentation Testing," International Journal of Solids and Structures, 49(14) pp. 1961-1972.

On establishing elastic–plastic properties of a sphere by indentation testing

J.K. Phadikar [a], T.A. Bogetti [b], A.M. Karlsson [a,*]

[a] Department of Mechanical Engineering, University of Delaware, Newark, DE, United States
[b] US Army Research Laboratory, Aberdeen Proving Ground, MD, United States

1. Introduction

Instrumented indentation has emerged as a valuable tool for probing elastic and plastic material properties of engineering materials (Cheng and Cheng, 2004; Green, 2005; Oliver and Pharr, 1992; Johnson, 1987; Jackson et al., 2010; Yan et al., 2007a, 2007b). During the experiment, a rigid indenter penetrates normally into a homogeneous solid, and the indenter force, P, and depth of penetration, h, are continuously measured during a complete cycle of loading and unloading. A typical force–displacement response is shown in Fig. 1. The force–displacement response is primarily a function of the elastic and plastic material properties of the substrate and the geometry of the indenter. Based on the force–displacement relationship and geometry of the substrate/indenter, the material properties of the substrate can be determined.

The most widely used method for determining elastic modulus for a flat semi-infinite substrate is the so-called "Oliver–Pharr method" (Oliver and Pharr, 1992). This method assumes that the initial unloading is elastic and thus uses the elastic solution for the problem to express the unloading slope in terms of elastic modulus, Poisson's ratio and contact radius (radius of projected area of contact at maximum depth of penetration). Accordingly, the relationship between the elastic properties of the substrate and the unloading slope is given by:

$$S = \left.\frac{dP}{dh}\right|_{h=h_{\max}} = 2\beta a \frac{E}{1-\nu^2} \tag{1a}$$

Here, S is the initial unloading slope, a is the contact radius at maximum load, $h_{\max}$ is the maximum depth of penetration, E and ν are elastic modulus and Poisson's ratio, respectively, of the substrate material, and β is a correction factor.

One disadvantage of this method is the need of the contact radius at maximum load, a, which is difficult to measure experimentally (Chen et al., 2006; Johnson, 1987). A common method to determine contact radius is to use the contact depth, δ_c, which can be determined from the following equation:

$$\delta_c = h_{\max} - \varepsilon \frac{P_{\max}}{S} \tag{1b}$$

Here, $P_{\max}$ is the force at maximum indentation depth, and ε is a dimensionless constant which depends on the indenter geometry, for example $\varepsilon = 0.75$ for a Berkovich indenter (Oliver and Pharr, 1992). However, this relationship is not valid in the case of plastic pile-up and thus not applicable to a range of cases (Cheng and Cheng, 2004; Pharr, 1998). Moreover, Eq. (1) does not give any information about the inelastic properties of the material. Due to these limitations, several authors have successfully used other aspects of the force-displacement relationship, including the indentation work during loading, elastic work recovered during unloading, residual depth, and force at maximum depth to determine the elastic and plastic properties (Cao and Lu, 2004; Xu and Li, 2005; Yan et al., 2007a, 2007b; Zhao et al., 2006).

* Corresponding author. Tel.: +1 302 832 6437l.
E-mail address: karlsson@udel.edu (A.M. Karlsson).

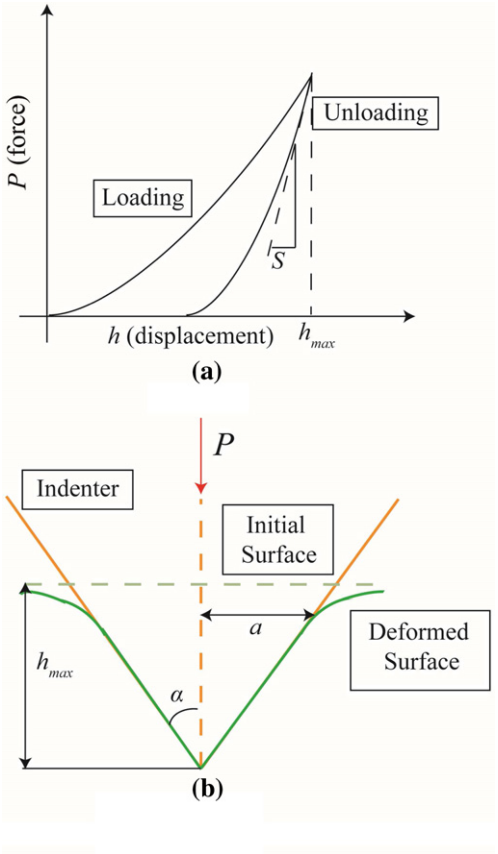

Fig. 1. (a) A typical force–displacement curve obtained in indentation experiments, and (b) the geometry of a conical indentation of a flat surface.

Instrumented indentation has become popular since the test is easy to conduct, and enables the establishment of mechanical properties for materials that only exist in small volumes. Currently, the literature on instrumented indentation is dedicated to indentation on flat surfaces, see for example reviews by Cheng and Cheng (2004) and by Oliver and Pharr (2004). However, not all small scale structures are flat. Examples of small scale spherical particles requiring material characterization include micron-sized metal coated polymer particles used in the manufacturing of anisotropic conductive adhesives (Kristiansen et al., 2001), and polymer latex particles for controlling the mechanical properties of latex films (Misawa et al., 1991; Tamai et al., 1989) used in the synthetic latex materials and living cells (Dao et al., 2003). The material properties are not affected by the geometry of the test specimen but the procedure to obtain material properties will vary according to the geometry of the substrate. Several authors have investigated the indentation of a hemi-sphere by a flat punch (Jackson and Green, 2005; Lin and Lin, 2006; Malayalamurthi and Marappan, 2008; Sahoo et al., 2009). However, to the knowledge of the authors, there are no studies in the open literature of a sphere indented by a conical indenter available. Thus, we aim to develop a reliable evaluation technique for conical indentation testing of spherical particles, schematically shown in Fig. 2. Note that the force–displacement response will retain the schematic features as shown in Fig. 1a.

2. Theoretical preliminaries

The indentation of a sphere ~~–~~ assumed to be made of linear-elastic, perfectly-plastic material is investigated. The sphere is resting on a rigid surface and the indenter is presumed rigid. Two

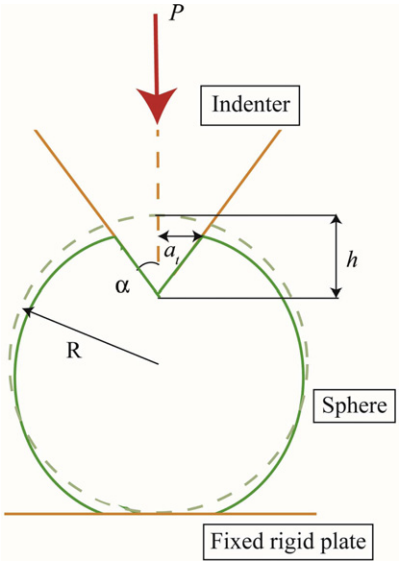

Fig. 2. Conical indentation of a sphere resting on a rigid flat surface indicating selected geometric parameters.

methodologies are proposed to determine the elastic and plastic material properties of the sphere, based on indentation testing. Both methods are founded on "reverse analysis." In reverse analysis, characteristic functions that link measurable structural behavior during the test sequence (e.g., unloading slope) to the material properties are first established. Then, when testing such a structure, the measurable quantities are recorded and used as input to the characteristic functions from where the material properties are extracted.

In the first method, the concept of elastic unloading is used. This method can be used to determine only the elastic modulus of the indented material. The characteristic function will be established via a mechanics based analytical approach. In the second method, a finite element based reverse analysis technique is utilized. To this end, numerical simulations of the indentation testing are conducted for a range of cases and characteristic, non-dimensional functions are identified and extracted from the simulations. These functions can then be used to extract elastic modulus and yield strength from a sphere subjected to indentation (real testing). Both methodologies will converge to indentation of a flat half-space when the maximum depth of penetration becomes very small compared to the radius of the sphere.

2.1. Elastic unloading

First, the concept of elastic unloading is explored as a tool for determining the elastic modulus of the indented sphere. To this end, we assume that the response is elastic during unloading (in a similar manner as Oliver and Pharr (1992)) and the instantaneous unloading slope achieved in the force–displacement diagram will be employed to extract the elastic modulus.

The concept of elastic unloading for flat surfaces can be summarized as follows. The classical Galin–Sneddon's solution for the force–displacement and contact depth–displacement relationship of a flat semi-infinite substrate indented by a rigid conical indenter is given by Galin (1961) and Sneddon (1965):

$$P = E_r \frac{2\tan\alpha}{\pi} h^2 \tag{2}$$

$$\frac{\delta_c}{h} = \frac{2}{\pi} \tag{3}$$

Here α is the indenter half-angle, δ_c is the contact depth, and E_r is the reduced modulus:

$$E_r = \frac{E}{1-\nu^2} \tag{4}$$

Based on the geometry (Fig. 1) the projected contact radius for a conical indenter can be expressed in terms of δ_c as:

$$a = \delta_c \tan\alpha \tag{5}$$

Oliver and Pharr (1992) assumed that unloading is elastic. This is a reasonable assumption, since unloading from a state of yielding results in an initial elastic response (Hill, 1998). For the current problem considered, the unloading slope can be established from Galin–Sneddon's force–displacement relationship (Galin, 1961; Sneddon, 1965). Differentiating Eq. (2) with respect to indentation depth, h, and utilizing Eqs. (3) and (5),

$$\frac{S}{E_r} = \frac{1}{E_r}\frac{dP}{dh}\bigg|_{h=h_{\max}} = 2a \tag{6}$$

Later, various correction factors have been introduced to the above relation by several authors to incorporate for example the effect of pile-up. For a concise description of the correction factors proposed by various authors, see the review by Oliver and Pharr (2004).

Inspired by this approach, we adopt the concept of elastic unloading of the sphere (of radius R) resting on a rigid flat surface and indented by a rigid conical indenter (of indenter half-angle α), Fig. 2. Similar to the Oliver–Pharr approach we propose that there exists a functional relationship between unloading slope, projected contact radius, a_t, and reduced elastic modulus:

$$\frac{S}{E_r} = F(a_t) \tag{7}$$

Eq. (7) simplifies to Eq. (6) where $F(a) = 2a$ for a flat surface. If the characteristic function F is known, the elastic modulus can be computed by determining S and a_t experimentally.

Assuming small and elastic displacements, the problem of a conical indenter indenting a sphere resting on a flat surface can be solved as superposition of two problems as shown in Fig. 3. The first part is a rigid cone–hemisphere contact problem where the bottom surface of the hemisphere is resting on a rigid surface (i.e., fixed) and the displacement of the conical indenter tip is h_c (Fig. 3b). The second part is a hemisphere-flat punch contact problem where the flat punch is fixed and the top surface of the hemisphere is displaced by h_s (Fig. 3c). Using Newton's second and third laws, it is evident that the indentation force P is acting on the two sub-problems as indicated in Fig. 3b and c. Using superposition, the overall displacement can be expressed as the sum of displacements of the two sub-problems, i.e., $h = h_c + h_s$. Solution for the first sub-problem, the elastic indentation of a hemisphere by a rigid conical indenter (Fig 3b), has been reported by Fu (2007):

$$a_c = -\frac{R}{4}\left[\pi\cot\alpha - \sqrt{(\pi\cot\alpha)^2 + \frac{16h_c}{R}}\right] \tag{8a}$$

$$P = E_r\left(2a_c h_c - \frac{\pi a_c^2\cot\alpha}{2} - \frac{2a_c^3}{3R}\right) \tag{8b}$$

To the knowledge of the authors, only two analytical solutions are available in the literature for the second sub-problem (a hemisphere subjected to loading via a flat punch). These are reported by Hertz (Johnson, 1987) and by Tatara (1989, 1991). Hertz's solution (Johnson, 1987) for this problem is given as:

$$a_b = \sqrt{h_s R} \tag{9a}$$

$$P = \frac{4}{3}E_r R^{1/2} h_s^{3/2} \tag{9b}$$

The Tatara's solution (Tatara, 1989, 1991) for this problem is given as:

$$a_b = \left[\frac{3RP}{4E_r}\right]^{1/3} \tag{10a}$$

$$h_s = \frac{3P}{4a_b E_r} - \frac{P}{\pi E_r}\left[\frac{1}{L} + \frac{2R^2}{L^3(1-\nu)}\right] \tag{10b}$$

$$L = \sqrt{a_b^2 + 4R^2} \tag{10c}$$

Hertz's solution is based on small displacement formulation whereas Tatara's solution is based on large displacement formulation. Thus, Tatara's solution is expected to be more accurate than Hertz's solution as the load (deformation) is increased.

Eqs. (8) and (10) do not lend themselves to be inverted analytically to form a closed-form solution. Consequently, the P–h relation of the complete system cannot be obtained analytically. However, using these relations, the following numerical algorithm is developed to establish the characteristic function defined in Eq. (7) for known values of sphere radius, R, and indenter half angle, α:

Step 1: Assume a value of the indentation depth for first sub-problem, h_c.
Step 2: Determine the contact radius, a_c, and the ratio P/E_r using Eq. (8).

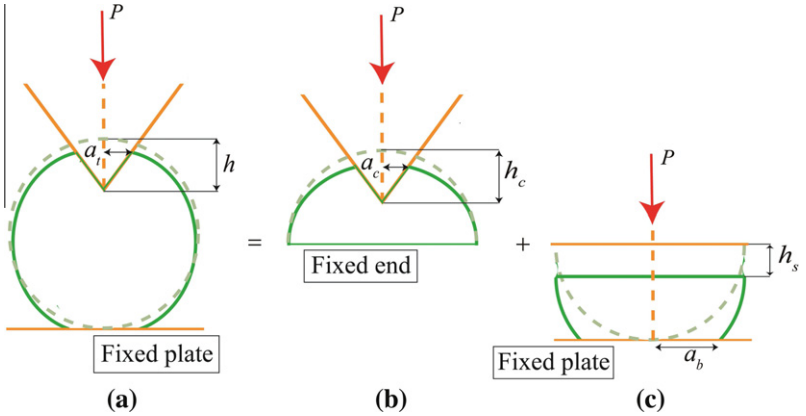

Fig. 3. Solving the cone–sphere contact problem via superposition: (a) the complete problem; (b) the upper half model; (c) the lower half model.

Step 3: Utilizing the computed value of P/E_r, determine the deformation of the hemisphere, h_s using Eq. (9) for Hertz's solution or Eq. (10) for Tatara's solution.
Step 4: Determine the total displacement of the sphere, $h = h_c + h_s$.
Step 5: Repeat Steps 1–4 with a value of indentation depth $h_c + \Delta h_c$ in Step 1 where Δh_c is a very small change in h_c. Thus, obtain $P/E_r + \Delta(P/E_r)$ from Step 2 and $h + \Delta h$ from Step 4.
Step 6: Determine S/E_r using the forward difference formula for numerical differentiation as $\Delta(P/E_r)/\Delta h$.
Step 7: Repeat Steps 1–6 for a range of values of h_c. Thus, obtain extended sets of S/E_r (from Step 6) and a_c (from Step 2) which can be used to develop an empirically established function $S/E_r = F(a_c)$.

If this algorithm is applied for indentation of a flat substrate in conjunction with Eqs. (2) and (5), it can be easily shown that Eq. (6) is obtained. This algorithm can also be used to determine the force–displacement relationship for the cone–sphere indentation problem of linear elastic materials, where the loading and unloading curves will be identical.

Ignoring plastic pile-up, Oliver and Pharr (1992) derived a formula (Eq. (1b)) to compute the contact depth and the projected contact radius (which is difficult to measure experimentally). However, a similar formula cannot as readily be derived for the present problem, thus imposing a limitation of the present methodology.

2.2. Functional forms from dimensional analysis

Next, a finite element based reverse analysis technique is utilized. To this end, numerical simulations of the indentation testing are conducted for a range of cases and characteristic, non-dimensional functions are identified and extracted from the simulations. These functions can then be used to extract elastic modulus and yield strength from a sphere subjected to indentation (real testing).

Dimensional analysis is widely used as a guideline for evaluating indentation testing and will be used here. Such an approach is used to reduce the computational cost involved with finite element simulations. Yan et al. (2007a) established a set of non-dimensional relations for conical indentation on a homogeneous, isotropic semi-infinite flat substrate, which can be expressed as

$$\frac{S}{Eh_{\max}} = f\left(\frac{E}{Y}\right) \tag{11}$$

$$\frac{W}{Yh_{\max}^3} = g\left(\frac{E}{Y}\right) \tag{12}$$

where f and g represent functions obtained from extensive numerical simulations. E and Y are the elastic modulus and yield strength, respectively, of the linear-elastic, perfectly-plastic material. $h_{\max}$ is the indentation depth at maximum load and W is the indentation work during loading i.e. $W = \int_0^{h_{\max}} P(h)dh$. Using a similar approach, and utilizing Buckingham's PI theorem (Buckingham, 1914) for indentation on a sphere, the following non-dimensional relations with functions Φ and Γ can be obtained:

$$\frac{S}{Eh_{\max}} = \Phi\left(\frac{E}{Y}, \frac{h_{\max}}{R}, \alpha\right) \tag{13}$$

$$\frac{W}{Yh_{\max}^3} = \Gamma\left(\frac{E}{Y}, \frac{h_{\max}}{R}, \alpha\right) \tag{14}$$

Here, the expressions are augmented to include the half angle α of the indenter tip. Poisson's ratio and the coefficient of friction are not included in these relations, as effects of these two parameters have been shown to be a minor factor during indentation testing (Cheng and Cheng, 1998, 2004; Hyun et al., 2011; Le, 2008; Mesarovic and Fleck, 1999). Thus, changing any of these two parameters will not result in considerable deviation in monitored indentation parameters (it will be shown in Section 6 that the methodology is moderately sensitive to experimental errors and consequently the sensitivity for these parameters cannot be resolved from indentation testing). Multiplying Eq. (13) by (E/Y) and Eq. (14) by (Y/E), two similar relations can be obtained as follows:

$$\frac{S}{Yh_{\max}} = \bar{\Phi}\left(\frac{E}{Y}, \frac{h_{\max}}{R}, \alpha\right) \tag{15}$$

$$\frac{W}{Eh_{\max}^3} = \bar{\Gamma}\left(\frac{E}{Y}, \frac{h_{\max}}{R}, \alpha\right) \tag{16}$$

Dividing Eq. (13) by Eq. (16) (or Eq. (15) by Eq. (14)) results in the following relation:

$$\frac{S}{W}h_{\max}^2 = \bar{\Theta}\left(\frac{E}{Y}, \frac{h_{\max}}{R}, \alpha\right) \tag{17}$$

The functional forms of the right hand sides of Eqs. (13)–(17) can be obtained from extensive finite element simulations and are characteristic functions of the indentation experiments.

The characteristic functions established above constitute a data reduction scheme which can be used to establish the elastic-plastic properties of a sphere. In particular, S, W, $h_{\max}$ and R are obtained from experiment and by using a subset of Eqs. (13)–(17), the material properties E and Y can be obtained, as will be discussed in Section 4.2.

3. Finite element model

In the present work, the finite element simulations were performed using the commercial finite element code ABAQUS (ABAQUS, 2009). The sphere is assumed to be composed of homogeneous, isotropic, linear-elastic, perfectly-plastic material with Poisson's ratio of 0.2. An axisymmetric, two-dimensional model was adopted and approximately 24,000 CAX4R elements were used to model the sphere. The sphere is assumed to rest on a flat rigid surface. Both the flat surface and the indenter are modeled as rigid bodies. Coulomb's friction law is used and the friction coefficient between the surfaces is taken to be 0.2 (Taljat et al., 1998). Several simulations with refined meshes and time increments (i.e., the step size of each simulation increment along the load path) were investigated for the convergence study.[1] The model used, shown if Fig. 4, gave the same results as a finer mesh and time increment. Thus, the selected refinement is sufficient to capture the mechanism of indentation. This model has been used for most of the simulations whereas slightly different meshes were adopted for simulating large indentation depth-to-radius ratios. The surface nodes of the sphere are traction free and the nodes along the axis of symmetry are constrained in the direction normal to indenter displacement to simulate symmetry conditions. The rigid surface at the bottom of the sphere is kept fixed in all three directions.

The model simulates the rigid indenter being pushed into the sphere to a predefined position, and then the indenter is removed. The reaction force as a function of indenter displacement is recorded continuously over the loading and unloading sequence, similar to a real indentation experiment. Based on the force–displacement relationships obtained, indentation work, W, and initial unloading slope, S, can be established. In all these cases,

[1] The selection of proper incremental step size is important due to the highly nonlinear nature of the problem, which involves nonlinear material properties, nonlinear geometry ("large deformations") and contact between two pairs of surfaces.

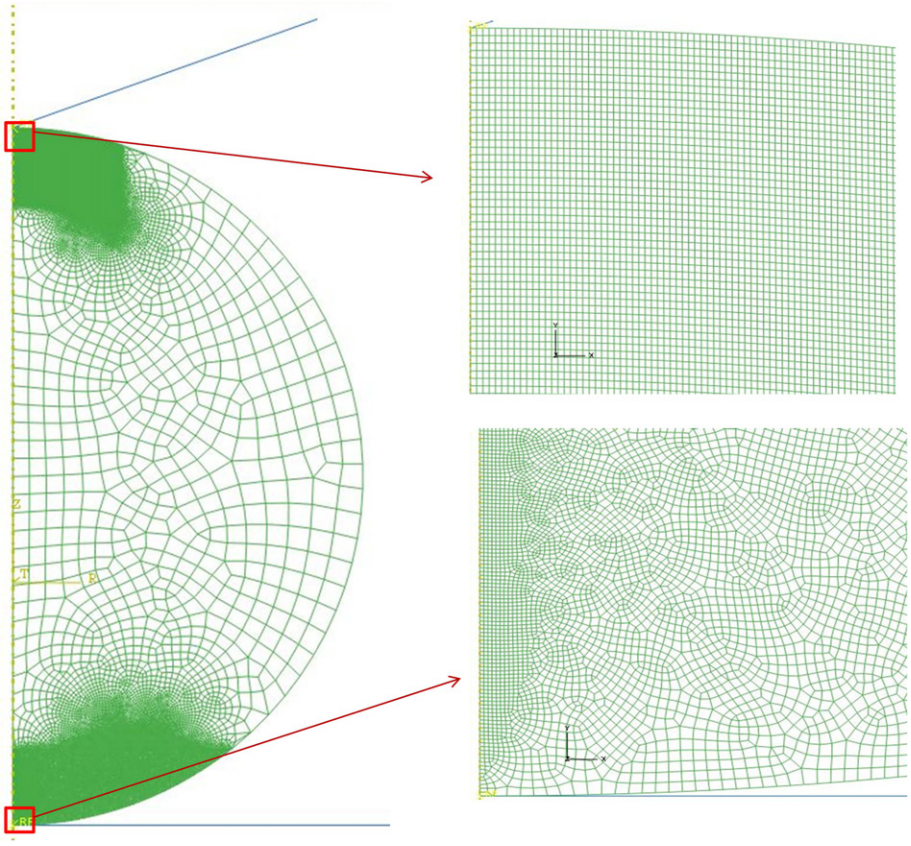

Fig. 4. Finite element model in ABAQUS, including enlargement of the refined mesh (plotted at the same scale) at the top of the sphere (conical indentation) and the bottom of the sphere (contact with the rigid surface).

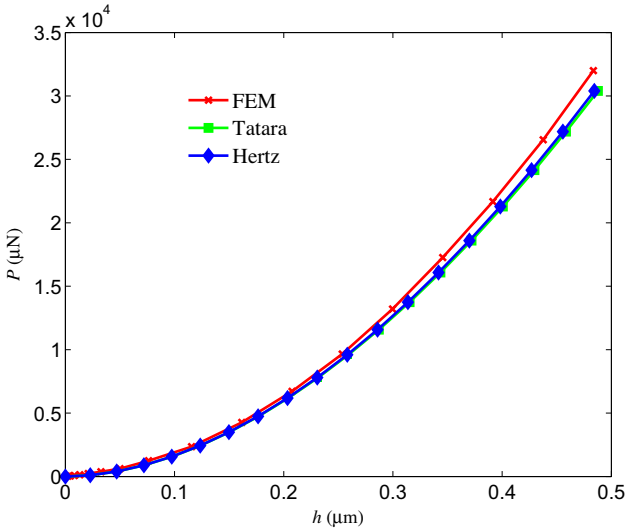

Fig. 5. Comparison of the force displacement response obtained using the finite element method and the superposition techniques. For a linear-elastic material (assumed here), the loading and unloading curves are identical.

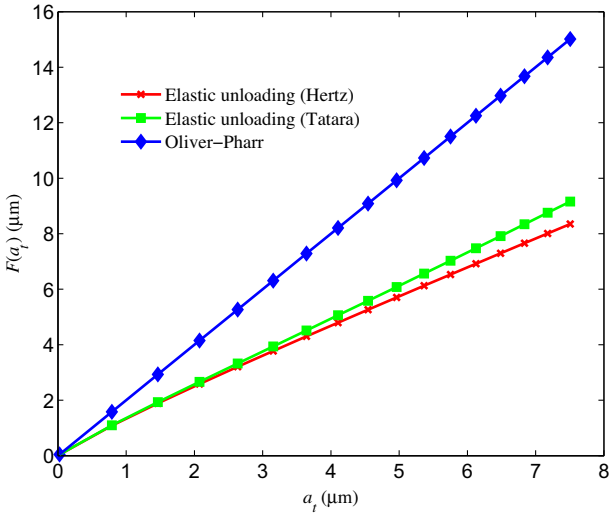

Fig. 6. The function $F(a_t)$ defined in Eq. (7) as function of a_t, the projected contact area for a 75° half-angle indenter indenting a sphere of radius 23 μm.

the initial unloading slope, S, was computed using the two points associated with the maximum load and 90% of the maximum load.

4. Establishing the functional forms

4.1. Elastic unloading

In Section 2.1, in order to determine the elastic modulus of the sphere, an algorithm based on utilizing the elastic unloading obtained from instrumented indentation was proposed. The algorithm is based on developing a relationship between the unloading slope, projected contact radius, and elastic modulus using a semi-analytical approach. Thus, an experimentally obtained unloading slope and projected contact radius can be used to determine the elastic modulus of the sphere. We will now discuss the functional forms obtained via this algorithm.

This algorithm provides the force–displacement relationship within the linear-elastic loading range for a sphere subjected to conical indentation. Thus, to investigate the viability of the algo-

rithm, we first compare the force-displacement response obtained from the algorithm (either using Hertz's relation or Tatara's relation for hemisphere-flat surface interaction) with results from finite element simulations. A sphere of radius 23 μm with elastic modulus 100 GPa and Poisson's ratio 0.2 is considered. The indenter half-angle is taken to be $\alpha = 75^\circ$. The force–displacement relation relationships are shown in Fig. 5. It can be seen that they are in good agreement with each other, where (within the resolution of the figure) the two analytical results overlap. Thus, the proposed algorithm appears to give reliable force-displacement relationships.

As discussed in Section 2.1, the proposed reversed analysis is based on developing a function, F, that relates the unloading slope $S = (dP/dh)|_{h=h_{max}}$, to the projected contact area, a_t, and the reduced modulus, E_r, as defined in Eq. (7). The function obtained by the proposed algorithm is shown in Fig. 6. If the "Oliver–Pharr method," Eq. (6), is used for this problem, it will predict $F(a_t) = 2a_t$ which is also shown in Fig. 6. Thus, it can be seen from the graph, and by using Eq. (7), that the Oliver–Pharr method will significantly under-predict the elastic modulus if it is used for evaluating indentation on a spherical substrate. The erroneous result is of course not a surprise, since that method is formulated to evaluate indentation of a flat surface. However, it can be seen that, for a given a_t, Hertz's model predicts a slightly smaller $F(a_t)$ compared to Tatara's model, and thus from Eq. (7), Hertz's model will predict slightly larger elastic modulus compared to Tatara's model. The accuracy of the present algorithm for predicting elastic modulus will be discussed later in this section.

4.2. Functional form from dimensional analysis

In Section 2.2, an algorithm based on characteristic, non-dimensional functions associated with the force–displacement relationships obtained during indentation testing was proposed as a data reduction scheme to establish elastic–plastic properties. These functions are obtained by conducting extensive finite element simulations, replicating indentation testing. The functional forms and the corresponding reverse analysis technique will be discussed in this section. With these functions established, the elastic modulus and yield strength can be determined from a sphere subjected to indentation testing (actual experiment).

To develop the functional forms presented in Eqs. (13)–(17), a material set with elastic modulus, E, and yield stress, Y, varying from 20 GPa to 220 GPa and 0.2 GPa to 0.8 GPa, respectively, was chosen to cover a wide range of E/Y ratios. For a 70.3° half angle indenter, the left hand sides of Eqs. (18) and (17) are plotted as a function of E/Y in Fig. 7, for three sets of (h_{max}, R) of constant $h_{max}/R = 0.05$. The procedure that was used to obtain the graphs is as follows:

Step 1: Select a set of materials with a range of E/Y ratios and obtain the force-displacement relationships for these materials for three sets of (h_{max}, R) of constant $h_{max}/R = 0.05$.
Step 2: From the obtained force-displacements relationships, determine S and W for each material and for each set of (h_{max}, R) and compute the left hand side of Eqs. (13)–(17) for these materials.
Step 3: Plot the left hand side of Eqs. (13)–(17) as functions of E/Y for three sets of (h_{max}, R).

Results from the algorithm above are plotted in Fig. 7(a–e) for three sets of of $h_{max}/R = 0.05$. Since the resulting curves in each graph overlap, it is clear that the results depend on the ratio h_{max}/R (rather than, for example, R). Thus, the assumption of using h_{max}/R as a non-dimensional quantity in Eqs. (13)–(17) is appropriate. The graphs presented in Figs. 7c and e correspond to Eqs. (15) and (17), respectively. These results indicate approximately linear responses and thus appear to be most suitable functional expressions to use in the reverse analysis. All other functional forms have significant regions with very low gradients within the range of investigated properties. That is, a large change in E/Y results in an insignificant change in the function, thus not being suitable as a base for the data reduction scheme.

Next, the functional forms for Eq. (15) and (17) will be determined explicitly. This is easily done by curve fitting the graphs obtained in Fig. 7. For simplicity, we assume a fixed indenter (i.e., constant half-angle, α) and various indentation depth-to-radius ratios. In this case, Eqs. (15) and (17) can be written as:

$$\frac{S}{Yh_{max}} = \phi_1\left(\frac{E}{Y}, \frac{h_{max}}{R}\right) \tag{18}$$

$$\frac{S}{W}h_{max}^2 = \theta_1\left(\frac{E}{Y}, \frac{h_{max}}{R}\right) \tag{19}$$

These functions can be determined for a particular value of α by extensive finite element simulations and surface fitting.

We now expand the functional forms to contain a range of h_{max}/R. Here, an indenter with $\alpha = 70.3^\circ$ half-angle is assumed, which represents the widely used Berkovich indenter.[2] A sphere of radius 23 μm was chosen and the range of $0.05 \leqslant h_{max}/R \leqslant 0.20$ was investigated. The numerical results are plotted in Fig. 8. The functional forms based on these results can be fitted as:

$$\frac{S}{Yh_{max}} = A_1\frac{E}{Y} + A_2 \tag{20a}$$

$$\frac{S}{W}h_{max}^2 = A_3\frac{E}{Y} + A_4 \tag{20b}$$

Here,

$$A_i = \sum_{j=0}^{5} a_{ij}\left(\frac{h_{max}}{R}\right)^{5-j}; \quad \text{for } i = 1, 2, 3, 4 \tag{20c}$$

The coefficients a_{ij} are tabulated in Table 1.[3]

Solving for E and Y, we get the following closed form equations relating E and Y with S, W, h_{max} and R:

$$E = \frac{S(Sh_{max}^2 - A_4W)}{h_{max}\{A_1(Sh_{max}^2 - A_4W) + A_2A_3W\}} \tag{21a}$$

$$Y = \frac{SA_3W}{h_{max}\{A_1(Sh_{max}^2 - A_4W) + A_2A_3W\}} \tag{21b}$$

Eq. (21) assumes a Berkovich indenter tip for a range of indentation depths. An alternative indentation test is to keep the ratio of indentation depth to radius fixed, and use various indenter half-angles. In this case, Eqs. (15) and (17) can be written as:

$$\frac{S}{Yh_{max}} = \varphi_2\left(\frac{E}{Y}, \alpha\right) \tag{22}$$

$$\frac{S}{W}h_{max}^2 = \theta_2\left(\frac{E}{Y}, \alpha\right) \tag{23}$$

[2] The Berkovich and conical indenter with half-angle 70.3° are equivalent since they have same projected contact area (Cheng and Cheng, 2004; Lichinchi et al., 1998). We assume that this equivalency holds for a substrate of any geometry including spherical substrate, at least within the range of deformations considered.

[3] In this case 20 coefficients are needed to describe the functions. This may seem like a large number of parameters, and we note that we are **not** striving to develop a relationship where the parameters can be interpreted as physical parameters, but we are just interested in finding "fitting parameters" that describe the intricate response. This method is commonly adopted in reverse analysis, see for example (Cao and Lu, 2004; Chen et al., 2006; Hyun et al., 2011; Le, 2008).

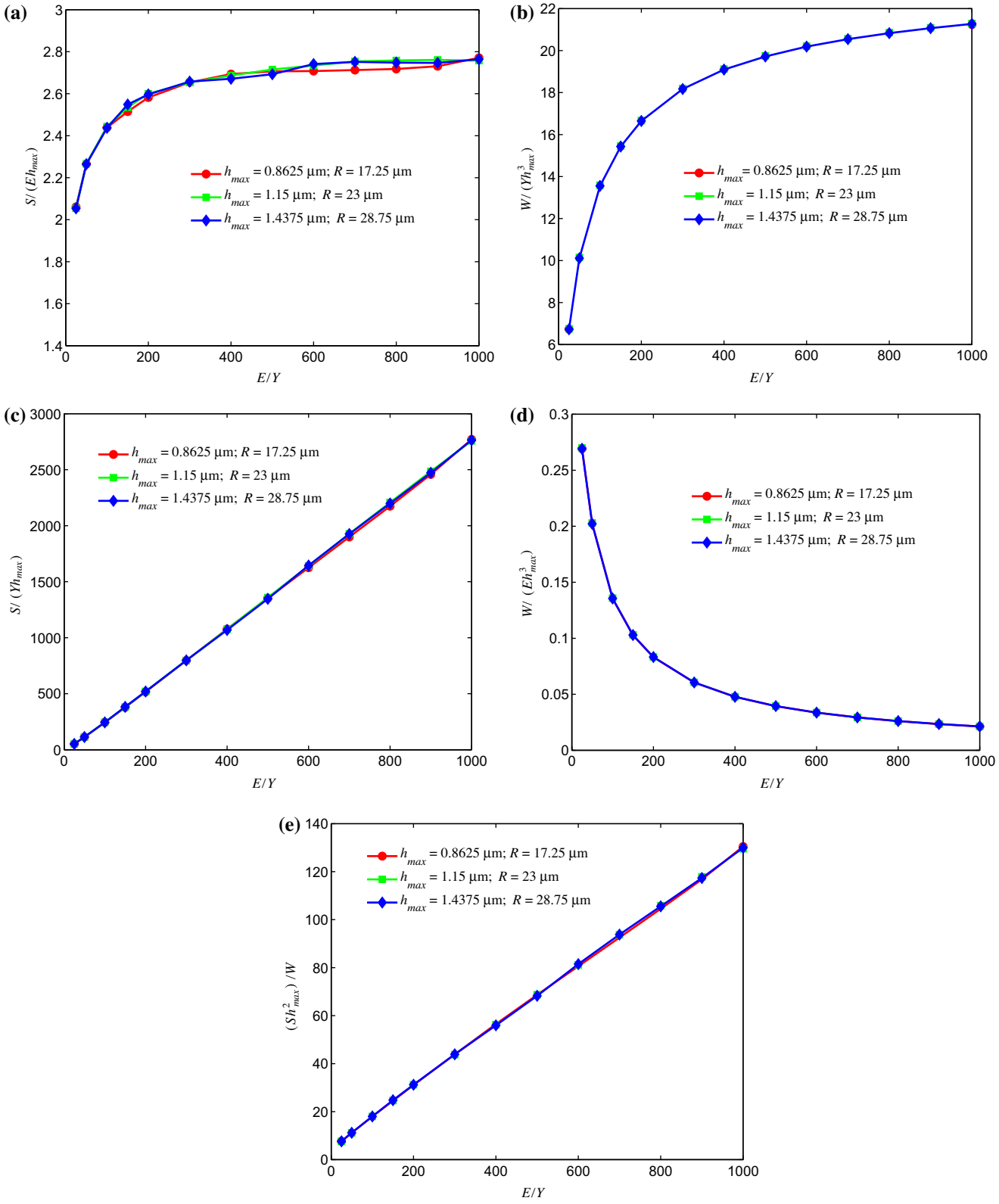

Fig. 7. Graphs of Eqs. (13)–(17) for $\alpha = 45^o$ of constant $h_{max}/R = 0.05$: (a) $\frac{S}{Eh_{max}} = \Phi(\frac{E}{Y}, \frac{h_{max}}{R}, \alpha)$, (b) $\frac{W}{Yh_{max}^3} = \Gamma(\frac{E}{Y}, \frac{h_{max}}{R}, \alpha)$; (c) $\frac{S}{Yh_{max}} = \bar{\Phi}(\frac{E}{Y}, \frac{h_{max}}{R}\alpha)$; (d) $\frac{W}{Eh_{max}^3} = \bar{\Gamma}(\frac{E}{Y}, \frac{h_{max}}{R}, \alpha)$; and (e) $\frac{S}{W}h_{max}^2 = \bar{\Theta}(\frac{E}{Y}, \frac{h_{max}}{R}, \alpha)$. It can be seen that the curves overlap within the resolution of the figure, indicating that h_{max}/R is an appropriate non-dimensional factor.

These functional forms can be determined using the previously described procedure except that in this case α is varied while h_{max}/R is kept constant. To elucidate this approach, a depth-to-radius ratio 0.10 was chosen and the range of indenter angle was set to $45^o \leqslant \alpha \leqslant 90^o$ to produce the characteristic functions in Eqs. (22) and (23). The numerical results are plotted in Fig. 9. The functional forms based on these results can be fitted as:

$$\frac{S}{Yh_{max}} = B_1\frac{E}{Y} + B_2 \qquad (24a)$$

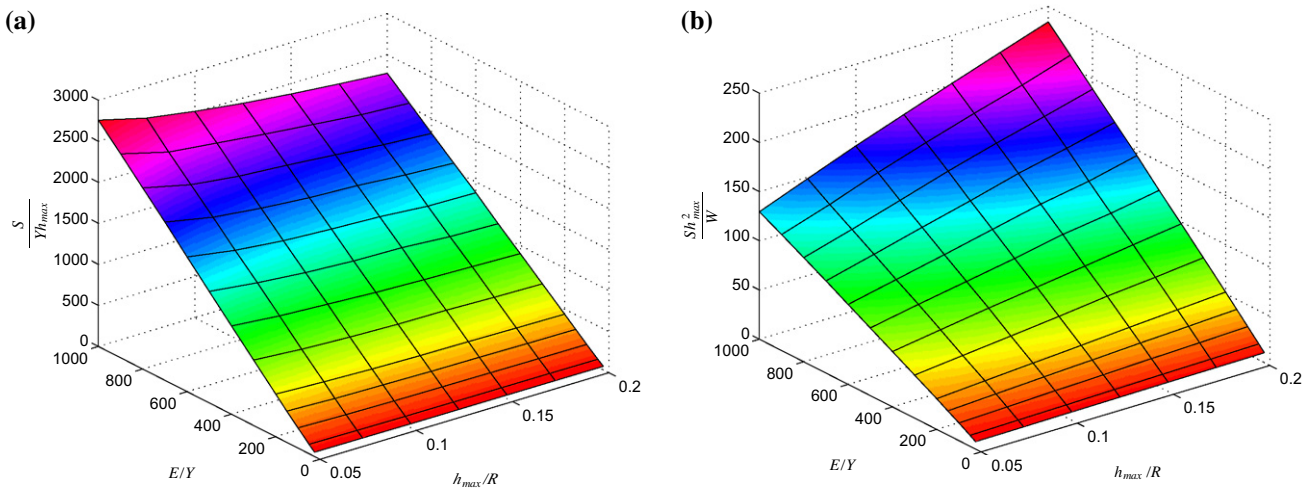

Fig. 8. Graphs of functions φ_1 and θ_1 of Eqs. (18) and (19) for $\alpha = 70.3°$ and $0.05 < h_{max}/R < 0.20$: (a) $\frac{S}{Yh_{max}} = \varphi_1(\frac{E}{Y}, \frac{h_{max}}{R})$ (b) $\frac{Sh^2_{max}}{W} = \theta_1(\frac{E}{Y}, \frac{h_{max}}{R})$.

Table 1
The coefficients a_{ij} used in Eq. (20c).

a_{ij}	$j = 0$	$j = 1$	$j = 2$	$j = 3$	$j = 4$	$j = 5$
$i = 1$	−8903.459	7831.082	−2594.525	413.2758	−34.64910	3.770216
$i = 2$	8,270,307	−5,379,602	1,335,208	−156,565.5	8676.3909	−211.6974
$i = 3$	278.3410	−77.16219	−6.997937	3.393041	0.4468455	0.09550578
$i = 4$	634,260.5	−409,015.8	100,461.3	−11,597.18	616.9314	−6.415562

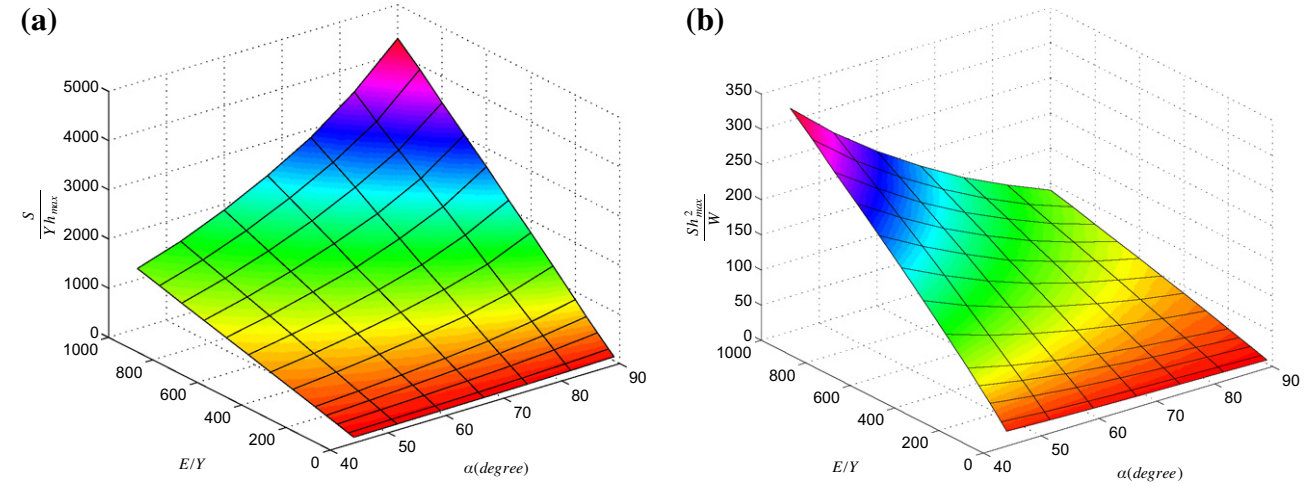

Fig. 9. Graphs of functions ϕ_2 and θ_2 of Eqs. (22) and (23) for $h_{max}/R = 0.10$ and $45° < \alpha < 90°$: (a) $\frac{S}{Yh_{max}} = \varphi_2(\frac{E}{Y}, \alpha)$ (b) $\frac{Sh^2_{max}}{W} = \theta_2(\frac{E}{Y}, \alpha)$.

$$\frac{S}{W}h_{\max}^2 = B_3\frac{E}{Y} + B_4 \qquad (24b)$$

where,

$$B_i = \sum_{j=0}^{5} b_{ij}\left(\frac{\pi\alpha}{180}\right)^{5-j}; \quad \text{for } i = 1,2,3,4 \qquad (24c)$$

and the coefficients b_{ij} are tabulated in Table 2.

Solving for E and Y, we get following closed form equations relating E and Y with S, W, h_{max} and R:

$$E = \frac{S(Sh_{\max}^2 - B_4W)}{h_{\max}\{B_1(Sh_{\max}^2 - B_4W) + B_2B_3W\}} \qquad (25a)$$

$$Y = \frac{SB_3W}{h_{\max}\{B_1(Sh_{\max}^2 - B_4W) + B_2B_3W\}} \qquad (25b)$$

The overall procedure for obtaining E and Y from an indentation experiment on a sphere is presented in a flowchart in Fig. 10.

Next, a procedure for the general case is presented. If it is not possible to conduct the indentation testing for the range of indentation depths or half-angles considered in the flowchart of Fig. 10 (for example, it might be required to do an indentation testing with $h_{max}/R = 15\%$ and $\alpha = 60°$), this procedure can be used. In this procedure, a finite element model needs to be built with experimentally used values of h_{max}, R and α. Since h_{max}, R and α are fixed, Eqs. (15) and (17) can be rewritten in terms of φ and θ as:

Table 2
The coefficients b_{ij} used in Eq. (24c).

b_{ij}	$j=0$	$j=1$	$j=2$	$j=3$	$j=4$	$j=5$
$i=1$	6.388084	−32.59418	66.00295	−64.13000	31.63645	−5.547653
$i=2$	−2098.035	12,211.78	−27,642.29	30,394.75	−16,291.38	3419.229
$i=3$	−0.0319618	0.2350247	−0.6716827	1.081783	−1.262186	0.8789901
$i=4$	−5.409768	10.34754	4.641567	6.113474	−56.41857	48.33569

$$\frac{S}{Yh_{\max}} = \varphi\left(\frac{E}{Y}\right) \tag{26}$$

$$\frac{S}{W}h_{\max}^2 = \theta\left(\frac{E}{Y}\right) \tag{27}$$

Once the functional forms are established from the finite element simulations, properties such as E and Y can be determined based on experimentally obtained values for S and W in the following steps:

Step 1: Determine the left hand side of of Eq. (27) from the experiments. Determine E/Y using function θ.

Step 2: Substitute the obtained value of E/Y into the function φ. As S and $h_{\max}$ are known from the experiments, calculate Y using Eq. (26).

Step 3**:** Using the obtained value of Y, compute E using the value of E/Y obtained in Step 1.

5. Numerical verification

At this time, no comprehensive experimental data are available (to the authors' knowledge) to verify the proposed scheme. Thus, we will use numerical simulations to investigate the validity of the proposed methods. Three sample materials (Yan et al., 2007a, 2007b) are used to verify numerically the proposed methodologies. The properties used for these materials were not used to develop the functional forms presented above.

Numerical simulations are conducted where the three sample materials are indented with an indenter with $\alpha = 70.3^{o}$. From these simulations (which acts as "numerical experiments"), the unloading slope, S, and the indentation work during loading, W, are extracted. The elastic modulus obtained using the method based on elastic unloading presented in Section 2.1 are tabulated in Table 3 along with the original input material properties. Hertz's solution predicts slightly higher elastic modulus than Tatara's solution. This is also expected from Fig. 6 and considering Eq. (7), since for a given value of a_t, the value of the function $F(a_t)$ predicted by Tatara's solution is slightly higher than predicted by Hertz's solution. The error in predicting elastic modulus lies within 12%. Moreover, the elastic modulus, E, and yield strength, Y, obtained using Eq. (21) based on the defining the functional forms of S and W via finite element simulations (the method proposed in Section 2.2), are also tabulated in Table 3. The proposed reverse analysis predicts the elastic modulus and yield strength quite accurately, with errors less than 3%.

In a similar manner, the accuracy of the proposed method is evaluated for a fixed depth-to-radius ratio of 0.10. The same sample materials are used in the finite element simulations to extract S and W for three selected indenter shapes. The half-angles that are chosen are 63.14^{o} (the cross-sectional area is half of that of the Berkovich indenter), 70.3^{o} (the cross-sectional area is same as the Berkovich indenter) and 75.79^{o} (the cross-sectional area is twice of that of the Berkovich indenter). The resultant E based on the method of elastic unloading, and E and Y obtained from Eq. (25), along with the original input material properties are tabulated in Table 4. It can be seen that also in this case, the proposed reverse analysis method predicts the values of E and Y quite accurately with errors less than 3% for the latter approach and the former with within 8% error.

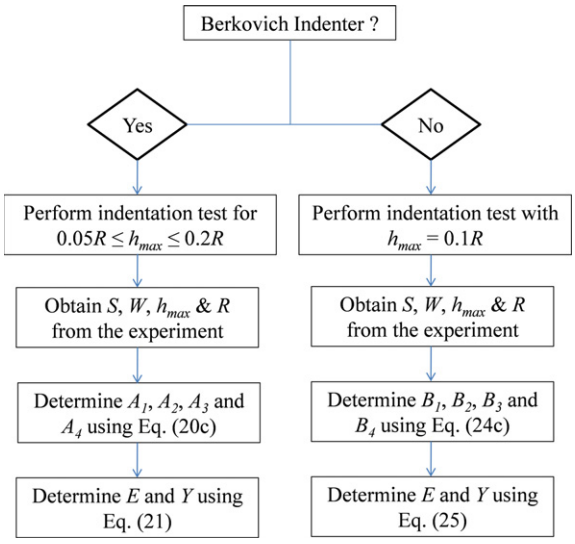

Fig. 10. Flowchart of the reverse analysis procedure.

6. Sensitivity analysis

Physical experiments always contain some degree of experimental error. To investigate the sensitivity of the proposed methodologies to such errors, we present a sensitivity analysis.

For the first method, i.e. the method based on elastic unloading, a sphere of radius 23 μm is indented numerically by a 70.3^{o} half-angle indenter with a maximum depth of penetration taken as 2.3 μm ($h_{\max}/R = 0.10$). The input material properties used are typical for bulk Ti–Al–Fe alloy and are assumed linear-elastic, perfectly-plastic. To examine the sensitivity of the algorithm based on elastic unloading with respect to unloading slope, S, and the projected contact radius, a_t, these two output parameters are varied within ±12% and corresponding errors obtained in calculated E are noted. It can be seen from Fig. 11 that for 12% difference in S or a_t, the percentage error in calculating E lies between 5% and 15% i.e. the same order of magnitude as the error imposed.

For the second method, a sphere of radius 23 μm is indented numerically by a 63.14° half-angle indenter with maximum depth of penetration as 2.3 μm ($h_{\max}/R = 0.10$). The input material is taken as typical properties for steel and linear-elastic, perfectly-plastic material is assumed. To examine the sensitivity of the algorithm developed based on non-dimensional functional forms with respect to unloading slope, S, and loading energy, W, these two output parameters are varied within ±12% and corresponding errors obtained in calculated (via the proposed evaluation techniques) E and Y are noted. It can be seen from Fig. 12 that the error in S does not affect the calculated value of Y considerably, whereas error in W does not affect the calculated value of E considerably. This may be expected since the unloading slope is determined from

Table 3
For selected indentation depths: Comparison of input material properties with that obtained using the functional forms based on elastic unloading (Section 2.1) and the finite element analysis (Section 2.2).

Input material properties	h_{max}/R	Elastic unloading		Functional form from FEA	
		Hertz E (% error)	Tatara E (% error)	E (% error)	Y (% error)
Bulk Ti	0.06	126 (3.08)	121 (6.92)	128 (1.54)	584 (2.67)
E = 130 GPa	0.11	135 (3.85)	127 (2.31)	129 (0.77)	588 (2.00)
Y = 600 MPa	0.16	145 (11.5)	133 (2.31)	129 (0.77)	591 (1.50)
Bulk Ti–Al–Fe	0.06	107 (2.73)	103 (6.36)	108 (1.82)	780 (1.89)
E = 110 GPa	0.11	115 (4.55)	109 (0.91)	109 (0.91)	780 (1.89)
Y = 795 MPa	0.16	122 (10.9)	113 (2.73)	108 (1.82)	784 (1.38)
Bulk steel	0.06	198 (5.71)	190 (9.52)	208 (0.95)	493 (1.40)
E = 210 GPa	0.11	219 (3.81)	204 (2.86)	209 (0.48)	495 (1.00)
Y = 500 MPa	0.16	232 (10.5)	214 (1.90)	209 (0.48)	497 (0.60)

Table 4
For selected half-angles of indentation: Comparison of input material properties with that obtained using the functional forms based on elastic unloading (Section 2.1) and the finite element analysis (Section 2.2).

Input material properties	Half-angle	Elastic unloading		Functional Form from FEA	
		Hertz E (% error)	Tatara E (% error)	E (% error)	Y (% error)
Bulk Ti	63.14	126 (3.08)	120 (7.69)	129 (0.77)	589 (1.83)
E = 130 GPa	70.3	134 (3.08)	127 (2.31)	129 (0.77)	587 (2.17)
Y = 600 MPa	75.79	140 (7.69)	131 (0.77)	128 (1.54)	585 (2.50)
Bulk Ti–Al–Fe	63.14	109 (0.91)	103 (6.36)	109 (0.91)	783 (1.51)
E = 110 GPa	70.3	113 (2.73)	107 (2.73)	109 (0.91)	779 (2.01)
Y = 795 MPa	75.79	119 (8.18)	112 (1.82)	108 (1.82)	779 (2.01)
Bulk steel	63.14	201 (4.29)	191 (9.05)	210 (0.00)	495 (1.00)
E = 210 GPa	70.3	215 (2.38)	202 (3.81)	210 (0.00)	495 (1.00)
Y = 500 MPa	75.79	225 (7.14)	211 (0.48)	209 (0.48)	494 (1.20)

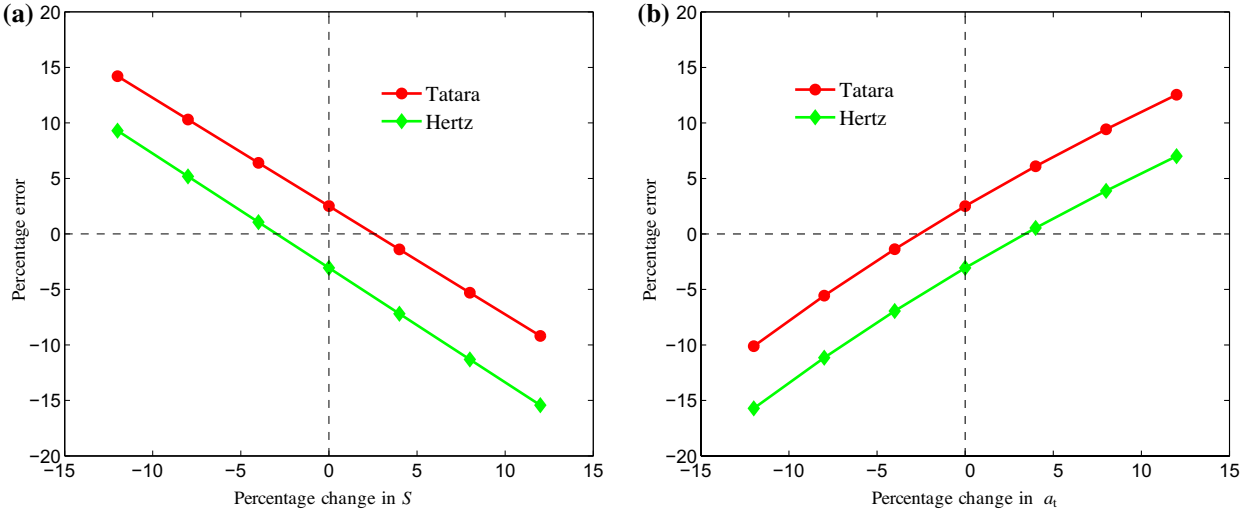

Fig. 11. Sensitivity in determining elastic modulus, E, with respect to imposing a small error in (a) the unloading slope, S, and (b) the projected contact radius, a_t, using the method based on elastic unloading.

the elastic unloading behavior and the loading work is governed by yielding. Further, it can be noted that for a 12% difference in S (or W) the percentage error in calculating E (or Y) lies between 10% and 15% i.e. the same order of magnitude as the error imposed.

7. Concluding remarks

In this paper, two methodologies based on reverse analysis are presented as a data reduction scheme to determine the elastic modulus and yield strength of a sphere via conical indentation. In both methods, functional forms are derived that relate output parameters from the indentation experiments to the elastic modulus and yield strength of the indented material.

In the first method, a relationship between the initial unloading slope, projected contact radius and elastic modulus is developed. The derivation is based on a semi-analytical approach and can be used to obtain the elastic modulus based the experimental data. By comparing the results obtained from the proposed method with

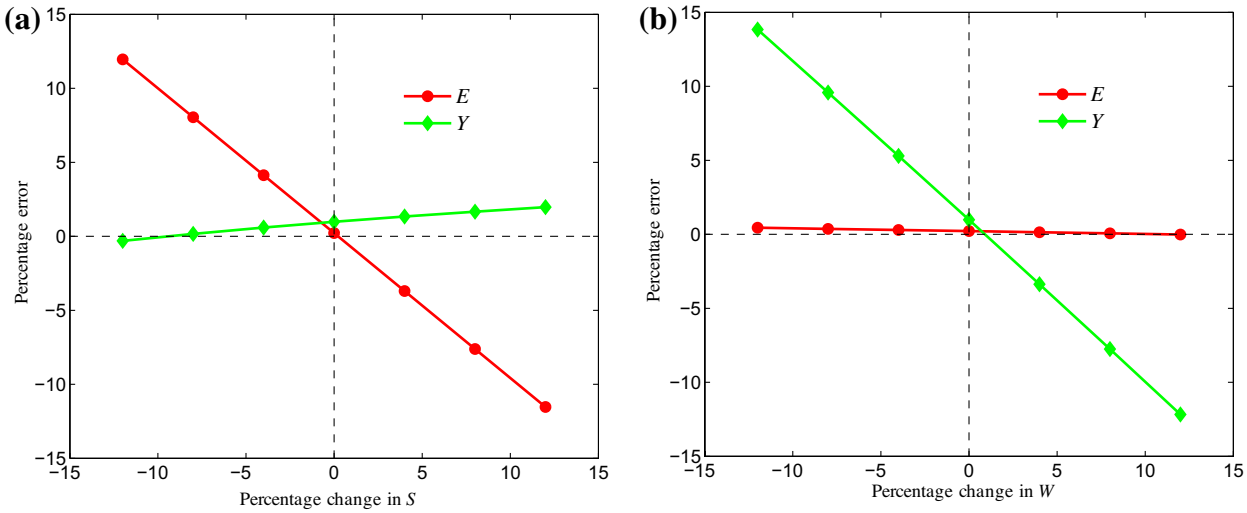

Fig. 12. Sensitivity in determining elastic modulus, E, and yield strength, Y, with respect to imposing a small error in (a) the unloading slope, S, and (b) the loading energy, W_t, using the method based on functional forms from non-dimensional groups.

results from finite element simulations, we show that this method predicts the elastic modulus with a less than 12% error. For comparison, the "Oliver–Pharr method" that is developed for flat surfaces will significantly under-predict the elastic modulus if it is applied for a sphere.

In the second method, dimensional analysis and finite element simulations are used to correlate governing characteristic functions, expressed in non-dimensional parameter groups, with material properties. For the particular scheme shown in this work using a Berkovich indenter, the experiment has to be performed by keeping the maximum indentation depth between 5% and 20% of the radius of the sphere whereas for a non-Berkovich indenter, the maximum indentation depth has to be kept at 10% of the radius. However, by following the proposed methodology the approach can be extended to any indenter geometry. By comparing the results obtained from the proposed method with results from finite element simulations, we show that this method predicts the elastic modulus and yield strength with a less than 3% error.

The sensitivity of the methodologies to experimental error was also investigated. In this case, the characteristic properties obtained from the (numerical) experiment were perturbed so to simulate experimental errors, and the properties predicted by the two methods were recorded. The results suggest that the error obtained when determining the material properties is of same order of magnitude of error in the experimental data. Thus, the method proposed is only moderately sensitive to experimental errors and – for the case of linear-elastic, perfectly-plastic materials – is therefore a viable data reduction method for conical indentation of spherical particles.

References

Abaqus Theory Manual, 2009. Version 6.9-2. Dassault Systèmes.

Buckingham, E., 1914. On physically similar systems; illustrations of the use of dimensional equations. Phys. Rev. 4, 345–376.

Cao, Y.P., Lu, J., 2004. A new method to extract the plastic properties of metal materials from an instrumented spherical indentation loading curve. Acta Mater. 52, 4023–4032.

Chen, X., Yan, J., Karlsson, A., 2006. On the determination of residual stress and mechanical properties by indentation. Mater. Sci. Eng. 416, 139–149.

Cheng, Y.T., Cheng, C.M., 1998. Scaling approach to conical indentation in elastic-plastic solids with work hardening. J. Appl. Phys. 84, 1284–1291.

Cheng, Y.T., Cheng, C.M., 2004. Scaling, dimensional analysis, and indentation measurements. Mater. Sci. Eng. R: Reports 44, 91–149.

Dao, M., Lim, C., Suresh, S., 2003. Mechanics of the human red blood cell deformed by optical tweezers. J. Mech. Phys. Solids 51, 2259–2280.

Fu, G., 2007. An extension of Hertz's theory in contact mechanics. J. Appl. Mech. 74, 373–374.

Galin, L.A., 1961. Contact problems in the theory of elasticity. In: Sneddon, I.N. (Ed.), North Carolina State Univ.

Green, I., 2005. Poisson ratio effects and critical values in spherical and cylindrical Hertzian contacts. Int. J. Appl. Mech. Eng. 10, 451–462.

Hill, R., 1998. The Mathematical Theory of Plasticity. Oxford university press.

Hyun, H.C., Kim, M., Lee, J.H., Lee, H., 2011. A dual conical indentation technique based on FEA solutions for property evaluation. Mech. Mater. 43, 313–331.

Johnson, K.L., 1987. Contact Mechanics. Cambridge university press.

Jackson, R.L., Green, I., Marghitu, D.B., 2010. Predicting the coefficient of restitution of impacting elastic-perfectly plastic spheres. Nonlinear Dynam. 60, 217–229.

Jackson, R.L., Green, I., 2005. A finite element study of elasto-plastic hemispherical contact against a rigid flat. J. Tribol. 127, 343–354.

Kristiansen, H., Shen, Y., Liu, J., 2001. Characterisation of mechanical properties of metal-coated polymer spheres for anisotropic conductive adhesive. IEEE, 344–348.

Le, M.-Q., 2008. A computational study on the instrumented sharp indentations with dual indenters. Int. J. Solids Struct. 45, 2818–2835.

Lichinchi, M., Lenardi, C., Haupt, J., Vitali, R., 1998. Simulation of Berkovich nanoindentation experiments on thin films using finite element method. Thin Solid Films 312, 240–248.

Lin, L.P., Lin, J.F., 2006. A new method for elastic-plastic contact analysis of a deformable sphere and a rigid flat. J. Tribol. 128, 221–229.

Mesarovic, S.D., Fleck, N.A., 1999. Spherical indentation of elastic-plastic solids. Proc. R. Soc. London A 455, 2707–2728.

Misawa, H., Koshioka, M., Sasaki, K., Kitamura, N., Masuhara, H., 1991. Three dimensional optical trapping and laser ablation of a single polymer latex particle in water. J. Appl. Phys. 70, 3829–3836.

Malayalamurthi, R., Marappan, R., 2008. Elastic–plastic contact behavior of a sphere loaded against a rigid flat. Mech. Adv. Mater. Struct. 15, 364–370.

Oliver, W.C., Pharr, G.M., 1992. An improved technique for determining hardness and elastic modulus using load and displacement sensing indentation experiments. J. Mater. Res. 7, 1564–1583.

Oliver, W., Pharr, G., 2004. Measurement of hardness and elastic modulus by instrumented indentation: advances in understanding and refinements to methodology. J. Mater. Res 19, 3–20.

Pharr, G., 1998. Measurement of mechanical properties by ultra-low load indentation. Mater. Sci. Eng. A 253, 151–159.

Sneddon, I.N., 1965. The relation between load and penetration in the axisymmetric Boussinesq problem for a punch of arbitrary profile. Int. J. Eng. Sci. 3, 47–57.

Sahoo, P., Chatterjee, B., Adhikary, D., 2009. Finite element based elastic–plastic contact behaviour of a sphere against a rigid flat – Effect of strain hardening. Int. J. Eng. Technol. 2, 1–6.

Tatara, Y., 1989. Extensive theory of force-approach relations of elastic spheres in compression and in impact. J. Eng. Mater. Technol. 111, 163–168.

Tamai, H., Hasegawa, M., Suzawa, T., 1989. Surface characterization of hydrophilic functional polymer latex particles. J. Appl. Polym. Sci. 38, 403–412.

Tatara, Y., 1991. On compression of rubber elastic sphere over a large range of displacements – Part 1: Theoretical study. J. Eng. Mater. Technol. 113, 285–291.

Taljat, B., Zacharia, T., Kosel, F., 1998. New analytical procedure to determine stress-strain curve from spherical indentation data. Int. J. Solids Struct. 35, 4411–4426.
Xu, Z.H., Li, X., 2005. Influence of equi-biaxial residual stress on unloading behaviour of nanoindentation. Acta Mater. 53, 1913–1919.
Yan, J., Chen, X., Karlsson, A., 2007a. Determining equi-biaxial residual stress and mechanical properties from the force-displacement curves of conical microindentation. J. Eng. Mater. Technol. 129, 200.
Yan, J., Karlsson, A., Chen, X., 2007b. Determining plastic properties of a material with residual stress by using conical indentation. Int. J. Solids Struct. 44, 3720–3737.
Zhao, M., Ogasawara, N., Chiba, N., Chen, X., 2006. A new approach to measure the elastic-plastic properties of bulk materials using spherical indentation. Acta Mater. 54, 23–32.